SCIENTIFIC REPORTS

OPEN

SUBJECT AREAS:
APPLIED PHYSICS
SURFACES, INTERFACES AND THIN FILMS
TWO-DIMENSIONAL MATERIALS
MAGNETIC PROPERTIES AND MATERIALS

Received
10 June 2013

Accepted
14 August 2013

Published
29 August 2013

Correspondence and requests for materials should be addressed to C.S. (songcheng@mail.tsinghua.edu.cn) or F.P. (panf@mail.tsinghua.edu.cn.)

# Strain engineering induced interfacial self-assembly and intrinsic exchange bias in a manganite perovskite film

B. Cui, C. Song, G. Y. Wang, H. J. Mao, F. Zeng & F. Pan

Key Laboratory of Advanced Materials (MOE), School of Materials Science and Engineering, Tsinghua University, Beijing 100084, China.

**The control of complex oxide heterostructures at atomic level generates a rich spectrum of exotic properties and unexpected states at the interface between two separately prepared materials. The frustration of magnetization and conductivity of manganite perovskite at surface/interface which is inimical to their device applications, could also flourish in tailored functionalities in return. Here we prove that the exchange bias (EB) effect can unexpectedly emerge in a (La,Sr)$MnO_3$ (LSMO) "single" film when large compressive stress imposed through a lattice mismatched substrate. The intrinsic EB behavior is directly demonstrated to be originating from the exchange coupling between ferromagnetic LSMO and an unprecedented $LaSrMnO_4$-based spin glass, formed under a large interfacial strain and subsequent self-assembly. The present results not only provide a strategy for producing a new class of delicately functional interface by strain engineering, but also shed promising light on fabricating the EB part of spintronic devices in a single step.**

Metal and semiconductor heterostructures have led to prominent advances in consumer electronics over the last decades[1–3]. Efforts are increasingly shifting to artificially constructed heterointerfaces between different complex oxides, accompanied by the observation of numerous fascinating phenomena, high-mobility conductivity[4,5], exchange bias[6,7], and ferroelectricity enhancement[8,9], etc. Among these oxide systems, the technological importance of magnetic tunnel junctions[10,11] and spin injectors[12] as potential applications of magnetically active mixed valence manganites, have continuously triggered extensive research.

The coupling of several degrees of freedom (such as spin, charge, lattice, and orbital) enriches the physical properties of mixed valence perovskite manganite[13]. Moreover, electrostatic and strain-related effects promote the electronic and structural reconstructions at interfaces among dissimilar oxides. Manganite films display very different properties, strongly affected by substrates and film thicknesses[14–16]. The existence of an interfacial layer (often referred to as the dead layer), which exhibits an insulating and non-ferromagnetic behavior, has been suggested to be responsible for the competitions between variable phases. The origin of this interfacial layer has been vigorously pursued and several mechanisms are proposed: electronic and/or chemical phase separation[16–18], $e_g$ orbital reconstruction and delocalization[19,20], and a $Mn^{3+}$ enrichment region[21], whereas a conclusive mechanism remains under debate. A long-term challenge for this rather contradictory situation is that the subtle variation at the interface makes its fingerprint hard to be directly detected. On the other hand, this interfacial layer is thought to be inimical to the device application[11,22]. Large amount of works are pursuing the reduction of dead layer through various ways like reducing the substrate/film lattice mismatch and changing interfacial chemical stoichiometry[23,24]. However, these attempts are so far incapable to completely eliminate the unfavorable structures[18]. Hence it is meaningful to go to the opposite direction, exploring a way to enlarge the interfacial reconstruction and benefit from it with tailored functionalities in return.

Specifically, the orbital reorganization results in an antiferromagnetic (AFM) layer in contrast to its ferromagnetic (FM) counterpart according to x-ray magnetic circular/linear dichroism (XMCD/XLD) experiments[16,19,21]. In-plane compressive or tensile epitaxial strain favours the $3z^2$-$r^2$ (C-type AFM) or the $x^2$-$y^2$ (A-type AFM) orbital ordering, respectively[16,19]. The EB effect, discovered 60 years ago[25] and now widely used in spintronic devices[2], is commonly observed in FM/AFM bilayers and its nature is still exploited[6,7,26]. It is then quite natural to expect an intrinsic exchange bias (EB) effect at the self-assembled FM/AFM interface, which is anticipated to enhance the spin polarization at FM/AFM interface and fabricate EB part of spintronic devices in a single step[22]. Although the AFM layer in manganite is depending on the $MnO_6$ octahedral distortion which could be tuned by the strain

engineering[27], the intrinsic EB effect observed in AFM-based manganites is still a question of interest lacking experimental insight and in-depth investigation[28–31].

In this context, to enlarge the compressive strain, $LaSrAlO_4$ (001) (LSAO; $a$ = 3.756 Å) substrates with a comparatively small lattice were intentionally employed to grow 45 unit cell (u.c.) $La_{2/3}Sr_{1/3}MnO_3$ (LSMO; $a$ = 3.870 Å for the bulk) films. The interfacial reconstruction of structure and composition is directly observed, resulting in two magnetic sublattices and intrinsic exchange bias in manganite. The structure evolution and property variation of different thickness LSMO also provides the growth dynamics for LSMO grown under large compressive strain.

## Results

A typical atomic resolution aberration-corrected high-angle annular dark field scanning transmission electron microscope (HAADF-STEM) image with its analysis is presented in Fig. 1. Remarkably, instead of a uniform film, the LSMO is divided into three sublattices in the order of increasing the distance from the film/substrate interface: (1) $LaAlO_3$-like (LAO-like), (2) $LaSrMnO_4$, and (3) LSMO. The boundaries and coherence (highlighted by colored spheres) of these three phases are clearly recognizable in the HAADF-STEM image. A magnified view of their schematic counterparts is illustrated in Fig. 1a. According to the electron energy-loss spectroscopy (EELS) ($d$ = 0.8 and 2.0 nm) and energy dispersive x-ray spectroscopy (EDX) with a spatial accuracy of one lattice site, it is surprisingly found that the film/substrate interface is a La and Al (diffused from the substrate during the 700°C growth) enrichment region (Supplementary Fig. S1a), in contrast to the lacking of Mn and depletion of Sr ascribed to the large compressive strain [the size of Sr (Mn) is much larger than that of La (Al)], exhibiting a chemical concentration far away from LSMO. A combination of concentration characterization and lattice feature with the thickness of 6 u.c., reveals the formation of $LaAlO_3$-like (LAO) layer just above the interface. It directly bears the strain from the substrate serving as a buffer layer.

The penetration of Sr and shortage of La (Fig. 1e,f) produce a $K_2NiF_4$ lattice in area (2) on the top of the LAO-like buffer. Taken together, concentration of this area and the LAO-like layer keeps a chemical equilibrium of LSMO. A closer inspection of the EELS results reveals that the Mn-$L_{2,3}$ spectrum in this area ($d$ = 3.2 nm) shifts to the low-energy comparing with those of the upper region, indicating that the valence of Mn is mainly in +3 (Ref. 32). The coexistence of $K_2NiF_4$ lattice in conjunction with enriched Sr and $Mn^{3+}$ demonstrate that a cell of AFM $LaSrMnO_4$ dominates in this area, followed by the growth of normal LSMO in area (3). This observation is corroborated by the inspection of O-EELS (Supplementary Fig. S1b) and surface sensitive XLD spectroscopy (Supplementary Fig. S2). In $LaSrMnO_4$, Mn ions at the corner of crystal cell share the $B$-site of LAO and LSMO, while La and Sr ions locate at its $A$-site, with $c$-axis of 13.09 Å. It is also reasonable to form self-assembled three phases in LSMO from the viewpoint of large lattice misfit between LSMO/LSAO, producing a lattice gradient of $a_{LSAO} < a_{LAO} < a_{LaSrMnO_4} < a_{LSMO}$ along the growth direction and the relaxation of large strain. Conversely, LSMO grown on $SrTiO_3$ substrate (the most used substrate for LSMO growth, $a$ = 3.904 Å) with a much smaller mismatch and a different sign of strain, exhibits a homogeneous film without obvious phase separation (Supplementary Fig. S3). A lattice distortion but without apparent self-assembly is observed in the LSMO film grown on $LaAlO_3$ ($a$ = 3.789 Å), which coincides with its moderate strain between the case on $LaSrAlO_4$ and $SrTiO_3$ (Supplementary Fig. S4), suggesting that the film/substrate interface could be tuned by strain. It is noteworthy that the LAO-like and $LaSrMnO_4$ phases constitute the dead layer of present LSMO film. In particular, magnetic frustration in the present interface is associated with a reconstruction of microstructure and composition, which is essentially different from the dead layer proposed previously[17–20], thus providing a new clue as to how to grow fascinating novel structures with tailored functionalities by the intentional interface design.

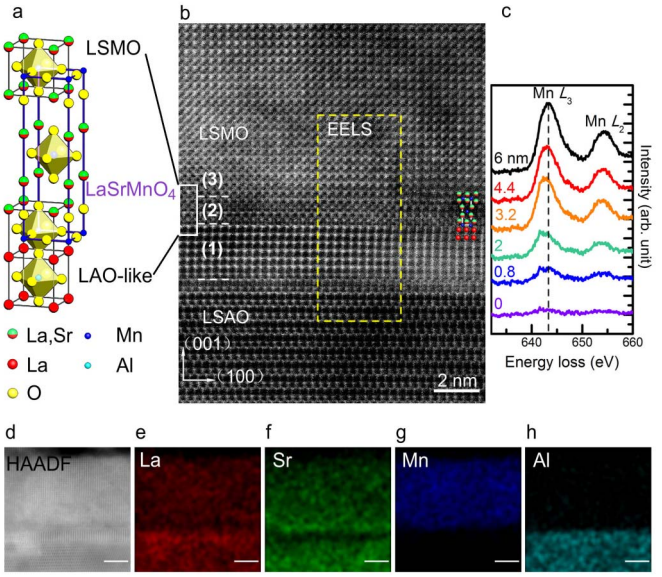


**Figure 1 | Direct observation of self-assembled structures in LSMO films.** (a), Sketch of LAO-like, $LaSrMnO_4$, and LSMO phases and their interfaces. (b), Typical HAADF-STEM image of the interfacial area. Interfaces between (1) LAO-like, (2) $LaSrMnO_4$ and (3) LSMO are marked by white dashed lines. The cations are highlighted by colored circles. (c), EELS Mn $L_{2,3}$ absorption edge for the region shown in the yellow frame of (b). The distance ($d$) in EELS is the space of the probing place and substrate surface, and the data are the average results of ±1 u.c. range. Elemental mappings by EDX measurement for the area of HAADF-STEM image (d) are shown in (e), La (red), (f), Sr (green), (g), Mn (blue), and (h), Al (cyan). The white scale bars in (d–h) represent a length of 5 nm.

Such unprecedentedly self-assembled structures have a profound influence on magnetic properties. Corresponding magnetic loops measured at 5 K are shown in Fig. 2a. One of the loops (solid sphere) was measured after field-cooling from room temperature in a +20 kOe field to 5 K. The most eminent feature observed here is the shift of the loop along the magnetic field axis towards negative fields (Fig. 2a). In contrast, on cooling in the presence of a −20 kOe field, the loop is biased in the positive direction. This observation confirms the presence of intrinsic EB in a nominally "single" LSMO film at low temperatures with a bias field $H_{EB}$ of 246 Oe, defined as the absolute offset of the loops along the field axis. These measurements are arbitrary from several subsequent runs with different growth that all confirm the reproducible EB behavior. The absence of biasing effect in LSMO grown on (001) $SrTiO_3$ (Supplementary Fig. S5) suggests the key role of considerable strain and layered structures for the exchange coupling. The blocking temperature ($T_B$) above which the symmetric magnetic loops are recovered independently of the cooling process, is of great importance for studying the strong coupling in LSMO. The dependence of the EB field on temperature is depicted in Supplementary Fig. S6 and summarized in Fig. 2b. The results of coercivity $H_C$ are also shown for a comparison. The EB field decreases with increasing the temperature, finally vanishing at around $T_B$ = 110 K. Also, the enhancement of $H_{EB}$ with the decrease of temperature indicates that the possible lateral phase separated LSMO, reduced in lower temperatures, should not be in charge of the EB effect observed[33–35]. This $T_B$ is self-consistent with the Néel temperature $T_N$ of $LaSrMnO_4$ of ~110K[14] and sets a temperature limit for the onset of the pinning activity for the AFM-based phase in LSMO. In general, $G$-type AFM $LaSrMnO_4$ could not contribute to

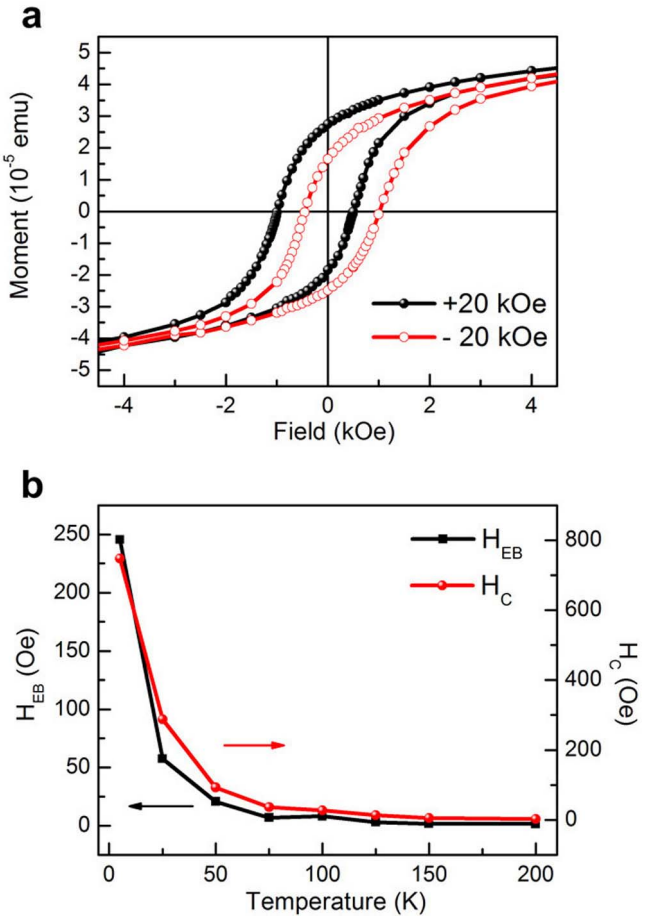


**Figure 2 | Intrinsic exchange bias in a LSMO "single" film.** (a), *M–H* loops of the 45 u.c. sample measured at 5 K after field cooling from room temperature in +20 kOe (solid spheres) and −20 kOe (open circles). For clarity, only the data between −4.5 and 4.5 kOe are shown in the figures, while the actual measurements were carried out between −20 and 20 kOe. (b), Temperature dependence of $H_{EB}$ and $H_C$ for the sample. The solid lines through the data points are guides to the eye.

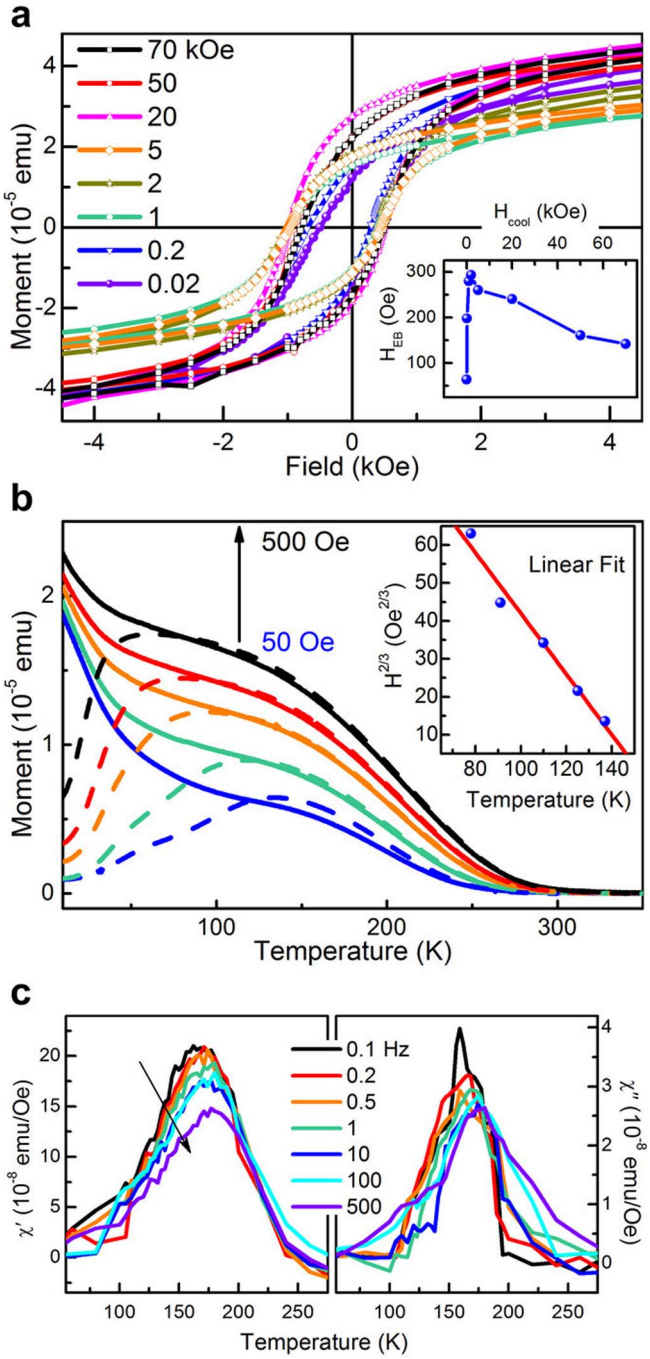


**Figure 3 | Demonstration of the LSMO/spin glass interface responsible for the exchange bias.** (a), *M-H* loops measured at 5 K after field cooling from room temperature in different magnetic fields of 0.02, 0.2, 1, 2, 5, 20, 50, and 70 kOe. $H_{EB}$ is shown as a function of the cooling field in the inset. (b), *M-T* curves measured under various fields ($H$ = 50, 100, 200, 300, and 500 Oe). The solid and dashed lines are the FC and ZFC data, respectively. The corresponding plot of $H^{2/3}$ vs $T_{irr}$ and linear fitting to Eq. (1) are shown in the inset. (c), Real χ' and imaginary χ″ ac magnetic susceptibility components at different frequencies as a function of temperature. The arrow indicates the shift of the maximum with increasing frequency and temperature.

the EB behavior because of its compensated spins arrangement[36,37], but recently spin canting[37] and the Dzyaloshinskii-Moriya interaction[38] are proposed to drive the exchange bias at FM/G-AFM interface. On the other hand, the monotonous decay of $H_C$ with temperature is different to some other known EB systems which have a peak at $T_B$[29]. It means that AFM-based phase in our case is not in a stable equilibrium, and the thermal effect strongly weakens its coupling with FM[7,36].

We now turn towards the unstable spin state in the AFM and the origin of EB effect. Hysteresis loops were measured at $T$ = 5 K, with various cooling fields ($H_{cool}$ = 0.02, 0.2, 1, 2, 5, 20, 50, and 70 kOe) (Fig. 3a). $H_{EB}$ as a function of $H_{cool}$ is subsequently summarized in the inset of Fig. 3a. We note that $H_{EB}$ increases rapidly to 293 Oe as $H_{cool}$ = 2 kOe, and then decreases monotonously to 142 Oe after cooling in a field of 70 kOe. Such a decrease of $H_{EB}$ under a large cooling field could be explained by the fact that the exchange coupling is reduced by the large Zeeman coupling[36,39]. This behavior normally occurs at a compensated AFM/FM interface associated with the interfacial canted AFM moments, which would be frozen at low temperatures[37,39–41]. The frozen state, most likely exists at $LaSrMnO_4$/LSMO interface in our system, is reaffirmed by the field-cooling (FC) and zero-field-cooling (ZFC) magnetization versus temperature (*M–T*) curves measured under various magnetic fields of 50, 100, 200, 300, and 500 Oe (Fig. 3b). There are two prominent features in the data: a peak in the ZFC *M–T* curves ($T_{peak}$) and a bifurcation between the ZFC and FC curves below the irreversibility temperature $T_{irr}$. These phenomena are quite characteristic for *M–T* curves involving spin glass[40]. Two characteristic temperatures ($T_{peak}$ and $T_{irr}$) are very close especially with a lower

measurement field, while both the $T_{peak}$ and $T_{irr}$ are reduced when the measurement field is enhanced, suggesting that the frozen state is clearly suppressed by a strong field. As presented in the inset of Fig. 3b, the dependence of $T_{irr}$ on the field follows the Almeida-Thouless line[40]:

$$H(T_{irr})/\Delta J \propto (1 - T_{irr}/T_F)^{3/2} \quad (1)$$

where $T_F$ is the zero-field spin glass freezing temperature and $\Delta J$ parameters the width of the distribution of the exchange interaction. The linear fit of the Almeida-Thouless line bolsters the existence of the spin glass behavior in LSMO with a freezing temperature $T_F \approx$ 147 K.

To further investigate the dynamics of spin glass in LSMO, ac susceptibility measurements were carried out in the range of 5–300 K with a field of 10 Oe and different frequencies (0.1–500 Hz), as presented in Fig. 3c. Apparently, frequencies dependent maxima are clearly recognizable for both the real (χ') and the imaginary (χ″) components of the magnetic susceptibility. Such maxima are intimately correlated to the frozen of moments with decreasing temperature[40,42]. As the frequency of the field is ramped up, the maxima become weaker and shift slightly to higher temperatures, which is due to the elongation of action time induced frozen delay[42]. The presence of spin glass as a result of magnetic frustration can be linked to the competition between the AFM super-exchange and the FM double-exchange interactions at the interface of $LaSrMnO_4$/LSMO[41]. We then conclude that the canted AFM moments associated with spin glass behavior is responsible for the EB effect.

Measurements performed over a range of LSMO thicknesses offer further insight into the EB effect and growth dynamics of self-assembled structures. A series of LSMO with different thicknesses on LSAO were then prepared. The EB behavior as a function of LSMO thickness is shown in Fig. 4a and its inset. The increase of film thickness to 45 u.c. boosts the $H_{EB}$ to the maximum of 246 Oe, and then $H_{EB}$ is reduced to 30 Oe for 150 u.c as expected, ascribed to the thick FM layer in the EB system[29]. Particularly, there is no resolvable exchange bias in fully strained 7 u.c. LSMO, indicating the absence of AFM phase in such ultrathin films. We confirm this speculation by a HAADF-STEM image and corresponding EDX results (Supplementary Fig. S7). Explanations may include that there is no lattice relaxation and space for phase separation in ultrathin films with several monolayers. At the initial growth stage (7 u.c.), the lattice volume of LSMO (53.4 Å$^3$) is much smaller than that of its bulk (57.9 Å$^3$), indicating the existence of a large compressive strain (Supplementary Fig. S8). Consequently, both the magnetism and conductivity are seriously suppressed, leading to a nonmetallic and weak-ferromagnetic LSMO with a low Curie temperature ($T_C$) of ~122 K, as shown in Fig. 4b and c. When the LSMO thickness increases, the lattice volume approaches to the value of the bulk, causing the monotonous enhancement of both $T_C$ and conductivity. The 45 u.c. LSMO sample shows a transition from a nonmetallic to metallic state considering the tendency of the temperature dependent resistivity. Nevertheless the thick samples, e.g., 150 u.c., show a much lower resistivity with a typical metallic state and $T_C \approx$ 310 K.

A comparison among the microstructures and physical properties of samples with different thicknesses, especially for the samples from 7 u.c. to 45 u.c., provides the growth dynamics for LSMO grown under large compressive strain as follows: initially a highly strained LSMO film is grown on LSAO showing a non-equilibrium state. Subsequently, both Mn and Sr are squeezed out by the interfacial strain, and the position of Mn is compensated by the diffusion of Al from the substrate, forming the LAO-like structure, above which AFM $LaSrMnO_4$ with one crystal cell emerges, and then it contacts with the FM LSMO with the formation of FM/spin glass interface. Both LAO-like and $LaSrMnO_4$ phases serve as buffer layers for the growth of normal LSMO, and most of the strain is released by these self-assembled structures. Differently, such interface engineering could not be observed in the LSMO deposited on $SrTiO_3$ (001) substrates due to the small film/substrate mismatch, whose strain energy could be released by a simple lattice distortion[16]. Correspondingly, we could not find any EB behavior for the LSMO with various thicknesses grown on the $SrTiO_3$ substrates (Supplementary Fig. S9), while for the films grow on $LaAlO_3$ (001) substrates the $H_{EB}$ are in between ($SrTiO_3$ and LSAO).

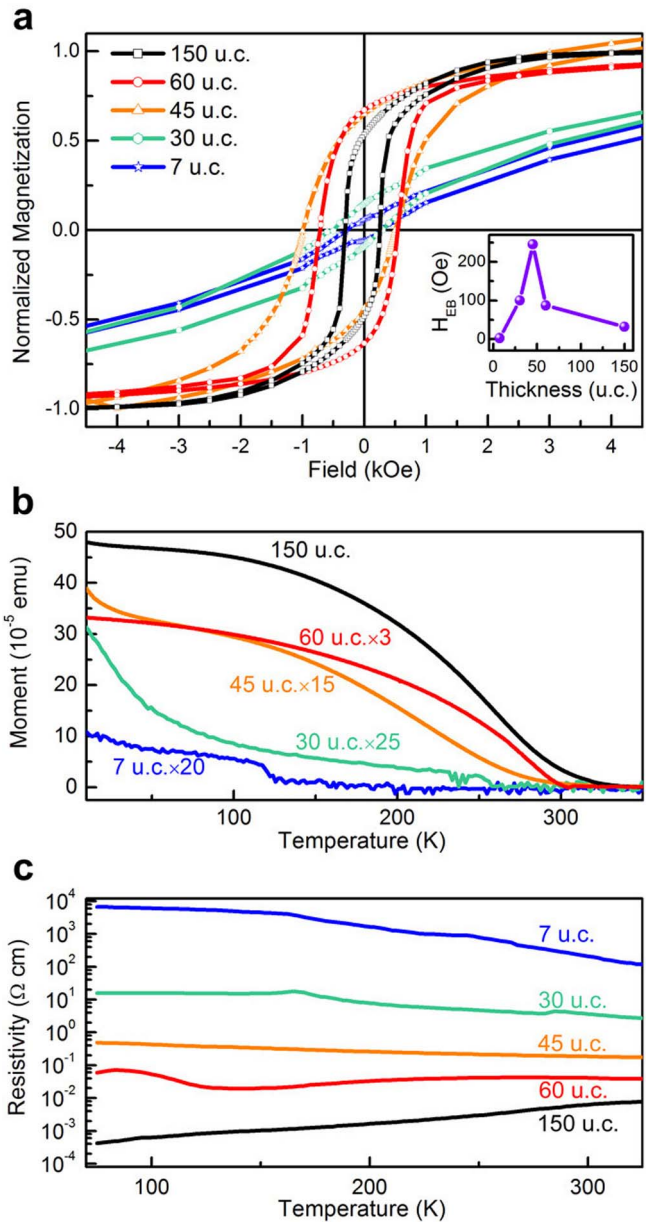


**Figure 4 | Magnetic and electric properties for LSMO samples with various thicknesses.** (a), Normalized *M-H* curves measured at 5 K after field cooling from room temperature in 20 kOe. *M-T* and *R-T* curves for different LSMO thicknesses (7, 30, 45, 60, and 150 u.c.) are presented in (b) and (c), respectively. For clarity, the moment in *M-T* curves are multiplied by a coefficient as shown.

## Discussion

The structural reconstruction of LSMO displays an enlarged image of interfacial state of manganite perovskite film, which might provide a new and in-depth understanding of the magnetic and electric frustration at the interface. The strain engineering design results in the formation of antiferromagnetic $LaSrMnO_4$ and ferromagnetic

LSMO interface through self-assembly in a nominally "single" LSMO film. The self-assembled structures with tailored functionalities that are inaccessible in uniform films include but not limited to the manganites. Hence this self-assembly and corresponding growth dynamics provide a conceptually novel vision for interface engineering on the growth of complex oxide films. The direct observation of antiferromagnetic phase near the interface and the intrinsic exchange bias derived from the coupling between LSMO/spin glass would advance the insight into the contradictory situation of the interface of LSMO. It paves a new way for investigating the dead layer and more studies are needed to fully understand the self-assembly and the exchange bias observed in manganite films. Besides its fundamental significance, the creation of a well-defined exchange bias system by self-assembly demonstrates the abroad ability for the fabrication of the biasing components of spintronics in a simplified way.

## Methods

**Sample preparation.** All of the samples were grown using pulsed layer deposition (PLD) from a stoichiometric $La_{2/3}Sr_{1/3}MnO_3$ target by applying a KrF excimer laser at a rate of 1.16 nm/min. During growth, the substrates ($LaSrAlO_4$, $SrTiO_3$, and $LaAlO_3$) were held at 700°C and in an oxygen background pressure of 200 mTorr. The growth was monitored in situ by RHEED (reflection high-energy electron diffraction) analysis allowing precise control of the thickness at the unit cell scale and accurate characterization of the growth dynamics (Supplementary Fig. S10a). After the growth, the samples were slowly cooled to room temperature in 300 Torr of oxygen at a rate of ~5°C/min to improve the oxidation level.

**Sample characterization.** Microstructures of cross-sectional samples were investigated by aberration-corrected HAADF-STEM in a Titan™ G2 80–200 with ChemiSTEM™ FEI with the resolution of 160 pm and 80 pm for image and probe corrector, respectively. EDX as well as EELS were performed with atomic resolution in order to probe the atomic structure of the interfaces and to check chemical interdiffusion. A Quantum Design superconducting quantum interference device (SQUID) measurement system (MPMS-7) was used to measure the magnetic properties in the temperature range 5–350 K with the magnetic field ($H$) applied in-plane along the (100) direction of the substrate. All the $M$–$H$ (magnetization versus magnetic field) and the field-cooling $M$–$T$ (magnetization versus temperature) measurements in this work without special statement were carried out after cooling down to 5 K in a magnetic field of 20 kOe and 2 kOe, respectively. Conductivity was determined in a Van der Pauw four-probe configuration by the ET9000 electric transport measurement system.


1. Hwang, H. Y. *et al.* Emergent phenomena at oxide interfaces. *Nature Mater.* **11**, 103–113 (2012).
2. Chappert, C., Fert, A. & Nguyen Van Dau, F. The emergence of spin electronics in data storage. *Nature Mater.* **6**, 813–823 (2007).
3. Hu, J. M., Li, Z., Chen, L. Q. & Nan, C. W. High-density magnetoresistive random access memory operating at ultralow voltage at room temperature. *Nature Commun.* **2**, 553 (2011).
4. Ohtomo, A. & Hwang, H. Y. A high-mobility electron gas at the $LaAlO_3/SrTiO_3$ heterointerface. *Nature* **427**, 423–426 (2004).
5. Herranz, G., Sánchez, F., Dix, N., Scigaj, M. & Fontcuberta, J. High mobility conduction at (110) and (111) $LaAlO_3/SrTiO_3$ interfaces. *Sci. Rep.* **2**, 758 (2012).
6. Wu, S. M. *et al.* Reversible electric control of exchange bias in a multiferroic field-effect device. *Nature Mater.* **9**, 756–761 (2010).
7. Gibert, M. *et al.* Exchange bias in $LaNiO_3$-$LaMnO_3$ superlattices. *Nature Mater.* **11**, 195–198 (2012).
8. Choi, K. J. *et al.* Enhancement of ferroelectricity in strained $BaTiO_3$ thin films. *Science* **306**, 1005–1009 (2004).
9. Rogdakis, K. *et al.* Tunable ferroelectricity in artificial tri-layer superlattices comprised of non-ferroic components. *Nature Commun.* **3**, 1064 (2012).
10. Bibes, M., Villegas, J. E. & Barthélémy, A. Ultrathin oxide films and interfaces for electronics and spintronics. *Adv. Phys.* **60**, 5–84 (2011).
11. Yamada, H. *et al.* Engineered interface of magnetic oxides. *Science* **305**, 646–648 (2004).
12. Barraud, C. *et al.* Unravelling the role of the interface for spin injection into organic semiconductors. *Nature Phys.* **6**, 615–620 (2010).
13. Dagotto, E. Complexity in strongly correlated electronic systems. *Science* **309**, 257 (2005).
14. Coey, J. M. D., Viret, M. & Molnár, S. von Mixed-valence manganites. *Adv. Phys.* **48**, 167–293 (1999).
15. Pesquera, D. *et al.* Surface symmetry-breaking and strain effects on orbital occupancy in transition metal perovskite epitaxial films. *Nature Commun.* **3**, 1189–1195 (2012).
16. Huijben, M. *et al.* Critical thickness and orbital ordering in ultrathin $La_{0.7}Sr_{0.3}MnO_3$ films. *Phys. Rev. B* **78**, 094413 (2008).
17. Dagotto, E., Hotta, T. & Moreo, A. Colossal magnetoresistant materials: the key role of phase separation. *Phys. Rep.* **344**, 1–153 (2001).
18. Kourkoutis, L. F., Song, J. H., Hwang, H. Y. & Muller, D. A. Microscopic origins for stabilizing room-temperature ferromagnetism in ultrathin manganite layers. *Proc. Natl. Acad. Sci. U.S.A.* **107**, 11682–11685 (2010).
19. Tebano, A. *et al.* Evidence of orbital reconstruction at interfaces in ultrathin $La_{0.67}Sr_{0.33}MnO_3$ films. *Phys. Rev. Lett.* **100**, 137401 (2008).
20. Lepetit, M. B., Mercey, B. & Simon, C. Interface effects in perovskite thin films. *Phys. Rev. Lett.* **108**, 087202 (2012).
21. Lee, J.–S. *et al.* Hidden magnetic configuration in epitaxial $La_{1-x}Sr_xMnO_3$ films. *Phys. Rev. Lett.* **105**, 257204 (2010).
22. Freeland, J. W. *et al.* Full bulk spin polarization and intrinsic tunnel barriers at the surface of layered manganites. *Nature Mater.* **4**, 62–67 (2005).
23. Sun, J. Z., Abraham, D. W., Rao, R. A. & Eom, C. B. Thickness-dependent magnetotransport in ultrathin manganite films. *Appl. Phys. Lett.* **74**, 3017 (1999).
24. Peng, R. *et al.* The origin of the dead-layer at the $La_{0.67}Sr_{0.33}MnO_3/SrTiO_3$ interface and dead-layer reduction via interfacial engineering. arXiv:1301.4822 (2013).
25. Meiklejohn, W. H. & Bean, C. P. New magnetic anisotropy. *Phys. Rev.* **102**, 1413–1414 (1956).
26. Wang, Y. Y. *et al.* Room-temperature perpendicular exchange coupling and tunneling anisotropic magnetoresistance in an antiferromagnet-based tunnel junction. *Phys. Rev. Lett.* **109**, 137201 (2012).
27. MacManus-Driscoll, J. L. *et al.* Strain control and spontaneous phase ordering in vertical nanocomposite heteroepitaxial thin films. *Nature Mater.* **7**, 314–320 (2008).
28. Niebieskikwiat, D. & Salamon, M. B. Intrinsic interface exchange coupling of ferromagnetic nanodomains in a charge ordered manganite. *Phy. Rev. B* **72**, 174422 (2005).
29. Karmakar, S. *et al.* Evidence of intrinsic exchange bias and its origin in spin-glass-like disordered $L_{0.5}Sr_{0.5}MnO_3$ manganites (L = Y, $Y_{0.5}Sm_{0.5}$, and $Y_{0.5}La_{0.5}$). *Phy. Rev. B* **77**, 144409 (2008).
30. Giri, S. K., Poddar, A. & Nath, T. K. Evidence of exchange bias effect and surface spin glass ordering in electron doped $Sm_{0.09}Ca_{0.91}MnO_3$ nanomanganites. *J. Appl. Phys.* **112**, 113903 (2012).
31. Xie, B. T., Zhao, Y. G. & Xiong, C. M. Capacitance characteristics of phase separated $La_{0.5}Ca_{0.5}MnO_3$/Nb–$SrTiO_3$ p-n junction. *Appl. Phys. Lett.* **93**, 072112 (2008).
32. Samet, L. *et al.* EELS study of interfaces in magnetoresistive LSMO/STO/LSMO tunnel junctions. *Eur. Phys. J. B* **34**, 179–192 (2003).
33. Becker, T. *et al.* Intrinsic inhomogeneities in manganite thin films investigated with scanning tunneling spectroscopy. *Phys. Rev. Lett.* **89**, 237203 (2002).
34. Tebano, A. *et al.* Strain-induced phase separation in $La_{0.7}Sr_{0.3}MnO_3$ thin films. *Phys. Rev. B* **74**, 245116 (2006).
35. Dagotto, E. *Nanoscale Phase Separation and Colossal Magnetoresistance* (Springer-Verlag, Berlin, 2003).
36. Kiwi, M. Exchange bias theory. *J. Magn. Magn. Mater.* **234**, 584–595 (2001).
37. Yu, P. *et al.* Interface ferromagnetism and orbital reconstruction in $BiFeO_3$-$La_{0.7}Sr_{0.3}MnO_3$ heterostructures. *Phys. Rev. Lett.* **105**, 027201 (2010).
38. Dong, S. *et al.* Exchange bias driven by the Dzyaloshinskii-Moriya interaction and ferroelectric polarization at $G$-type antiferromagnetic perovskite interfaces. *Phys. Rev. Lett.* **103**, 127201 (2009).
39. Bianco, L. Del *et al.* Field-cooling dependence of exchange bias in a granular system of Fe nanoparticles embedded in an Fe oxide matrix. *Phys. Rev. B* **70**, 052401 (2004).
40. Binder, K. & Young, A. P. Spin glasses: Experimental facts, theoretical concepts, and open questions. *Rev. Mod. Phys.* **58**, 801–976 (1986).
41. Ding, J. F. *et al.* Interfacial spin glass state and exchange bias in manganite bilayers with competing magnetic orders. *Phys. Rev. B* **87**, 054428 (2013).
42. Alonso, J. *et al.* Crossover from superspin glass to superferromagnet in $Fe_xAg_{100-x}$ nanostructured thin films ($20 \leq x \leq 50$). *Phys. Rev. B* **82**, 054406 (2010).


## Acknowledgements

The authors are grateful to Prof. Z. Zhang, Z. J. Shen, J. H. Hong of Zhejiang University for the assistance of TEM characterization, and to Prof. G. A. Gehring and Prof. P. Yu for fruitful discussions and critical reading of manuscript. The authors also acknowledge Beamline BL08U in Shanghai Synchrotron Radiation Facility (SSRF) for XLD measurements. This work was supported by the National Natural Science Foundation of China (Grant Nos. 51322101, 51202125 and 51231004), National Basic Research Program of China (Grant No. 2010CB832905) and National Hi-tech (R&D) project of China (Grant no. 2012AA03A706).

## Author contributions

B.C. and G.Y.W. prepared the samples. B.C. and C.S. carried out the measurements. C.S. and F.P. conceived and directed the project. F.Z. and H.J.M. provided advice on the experiments. All authors participated in discussing the data and writing the manuscript.

## Additional information

**Supplementary information** accompanies this paper at http://www.nature.com/scientificreports

**Competing financial interests:** The authors declare no competing financial interests.

**How to cite this article:** Cui, B. *et al.* Strain engineering induced interfacial self-assembly and intrinsic exchange bias in a manganite perovskite film. *Sci. Rep.* **3**, 2542; DOI:10.1038/srep02542 (2013).